Jürgen Ulpts, Wolfgang Dreher, Miriam Klink, Jorg Thöming

NMR imaging of gas phase hydrogenation in a packed bed flow reactor

NMR imaging of gas phase hydrogenation in a packed bed flow reactor

Jürgen Ulpts [a], Wolfgang Dreher [b,*], Miriam Klink [c], Jorg Thöming [a]

[a] Center for Environmental Research and Sustainable Technology (UFT), University of Bremen, Leobener Str. 1, 28359 Bremen, Germany
[b] University of Bremen, Department of Chemistry (FB2), In Vivo MR Group, Leobener Strasse, 28359 Bremen, Germany
[c] University of Bremen, Department of Chemistry (FB2), Institute of Applied and Physical Chemistry, Leobener Str., Germany

ARTICLE INFO

Article history:
Received 7 April 2015
Received in revised form 11 June 2015
Accepted 12 June 2015
Available online 22 June 2015

Keywords:
MRI gas measurements
Heterogeneously catalyzed gas phase reactions
Non invasive measurements of chemical composition
Fixed bed reactor
Ethylene hydrogenation
Multislice magnetic resonance spectroscopic imaging

ABSTRACT

In situ analysis of heterogeneously catalyzed gas phase reaction systems is becoming a valuable aid to their modeling and optimization. The commonly applied methods are either invasive, do not provide spatial information or are not applicable for optically inaccessible systems. This work investigates the possibility to use NMR imaging to study gas phase reaction processes in situ, spatially resolved and non-invasively.

A multislice NMR spectroscopic imaging pulse sequence, which was optimized to realize ultrashort echo time TE, was employed to study the ethylene hydrogenation reaction in an NMR-compatible packed bed flow reactor. The catalyst bed, containing inactive γ-Al_2O_3 pellets and Pt-Al_2O_3 pellets, was subdivided into several sections in order to identify reaction zones that depend on initial conditions. Spatial mapping of the chemical composition was demonstrated on the basis of two experiments with varying initial volume flow and ethylene conversion. The inlet and outlet temperature of the catalyst bed was simultaneously detected by analyzing the spectra of inserted glycol capsules.

The resulting spatial shift of the reactive zones in both experiments could be proven by the spatially resolved concentration measurements and the temperature measurements. The locations of single active catalyst pellets were also detectable by the same measure. The quantitative results of product gas composition of both experiments were in good agreement with accompanying mass spectrometric measurements.

The results demonstrate the applicability of NMR imaging methods to investigate gas phase reaction processes and can help to establish these methods as a standard tool to map chemical transformations in gas flow reactors.

1. Introduction

Heterogeneously catalyzed gas phase reactions have a substantial relevance for the chemical and energy industry. Prominent examples are the Sabatier reaction, the hydrogenation of alkines, the partial oxidation of alkenes or the oxidative dehydrogenation of alkanes. Due to the high potential of these reactions, performance enhancements of these processes are of high interest as even small improvements can already be economically viable [1].

A well established way to achieve significant enhancements is to optimize mass and heat transport within a catalyst bed, which are known to influence parameters like activity and selectivity drastically [2–5]. To optimize the processes within a reactor, knowledge about the inner conditions of a reactor is needed. However, techniques that provide integral information about chemical composition like online gas chromatography (GC) analysis or invasive measurements like probe thermometers, which provide a rather coarse spatial resolution at selected positions, are still state-of-the-art and are widely used to validate modeling approaches [6–8]. While these methods have clearly proven their value, methods which allow to non-invasively obtain information about temperature and chemical composition combined with high spatial and temporal resolution have gained considerable attention [9–13]. These methods are particularly suitable for the investigation of microscopic processes, such as adsorption reactions and the determination of reaction intermediates. However, the investigated reaction systems have to be optically accessible, which makes these methods not applicable when information about reaction processes within opaque environments, like porous catalyst beds, should be acquired.

Another approach to map chemical compositions and temperature, particularly in optically opaque reactors, is to apply nuclear magnetic resonance (NMR) based methods, i.e. magnetic resonance imaging (MRI), localized NMR spectroscopy (MRS) or magnetic

* Corresponding author.
E-mail address: wdreher@uni-bremen.de (W. Dreher).

http://dx.doi.org/10.1016/j.apcata.2015.06.011

resonance spectroscopic imaging (MRSI) [14,15]. These NMR based methods are not only well established and widely used diagnostic tools for medical and biomedical applications, but have also found various applications in material sciences and chemical engineering [16]. NMR based methods offer a lot of advantages compared to other methods. They are not only non-invasive, but additionally provide a whole realm of contrast mechanisms such as concentration, relaxation times, flow, diffusion, temperature or magnetization transfer. In particular, they allow to simultaneously measure parameters like chemical composition and temperature with both high spatial and temporal resolution, which is crucial to validate spatially resolved simulations of catalytic reactors.

Nowadays, suitable NMR imaging systems are widely available, although often in research facilities focusing on biomedical research, and not on material sciences or catalysis. Thus, MRI and MRSI might appear to be ideal tools to non-invasively investigate macroscopic transport processes within chemical reactors in situ. However, scientific publications on this topic are still rather rare, which is due to several reasons:

(i) A reactor designed for operation within an MRI magnet has to be made of NMR-compatible materials. The use of metals is limited, even if non-magnetic, as they would distort the static magnetic field B0 and/or screen the radio frequency (RF) field B1, thus making MRI measurements impossible. Therefore, the design of NMR compatible reactors is challenging, particularly for high temperature and high pressure.
(ii) The interaction between molecules of liquids or gases, which are to be measured, and the porous carrier material with the catalyst shortens the effective transverse relaxation time T2*. Thus the transverse magnetization decays rapidly after RF excitation, resulting in a decreased signal-to-noise ratio (SNR). Additionally, short T2* values require to apply strong and rapidly switchable B0 gradients for spatial resolution as well as optimized pulse sequences with ultrashort echo time (TE), i.e. an ultrashort delay between RF excitation and signal detection.
(iii) NMR is an inherently insensitive method with respect to SNR, e.g., as compared to mass spectrometry. This fact limits the detection of samples with low concentration of NMR active nuclei as well as the achievable spatial resolution. Solutions to this problem comprise the use of hyperpolarization [17,18] or special detection techniques such as “remote detection” [19,20].
(iv) Most of the suitable modern NMR imaging systems are available in a biomedical research environment and not in engineering departments. Considering the difficulties mentioned above and the high prices of NMR imaging systems, initial MRI or MRSI experiments for characterizing catalytic reaction will most likely require a multidisciplinary cooperation. However, this may be difficult to establish because of the considerable experimental requirements and the remaining risks of such projects.

Nevertheless, excellent work on investigating 3-phase reaction systems with MRI methods has been published, e.g., on octene hydrogenation and alpha-methylstyrene hydrogenation [21–25]. Furthermore, a method using the temperature dependence of chemical shift difference between the two signals of ethylene glycol, well known from high resolution NMR spectroscopy [26], was adapted for temperature measurements within an NMR compatible reactor [27]. Even gas phase reactions were investigated by using hyperpolarization or remote detection techniques [28–30]. Recently, an investigation of ethylene polymerization at industrial conditions in a specially designed NMR compatible reactor has been reported [31].

Along with the general requirements for investigating reaction processes by NMR based methods, the analysis of gas phase reactions provides further challenges [32,33]. The signal intensity of gases is much lower than the intensity of liquids because of the lower spin density (factor ~1000), especially at low pressure and high temperature. The spin-spin relaxation times T2 of gases are rather short, which decreases the SNR and complicates signal detection. Additionally, the short T2 and T2* relaxation times as well as the much higher diffusion constants of gases as compared to liquids hamper spatial encoding achieved by spatially selective RF pulses, phase encoding B0 gradients or readout B0 gradients.

To address these problems, this work investigates the possibilities to apply NMR based methods to heterogeneously catalyzed gas phase processes within reactors of conventional dimensions at ambient reaction conditions. It was the aim of this study to provide a methodology for observing chemical reactions and temperature changes in a rather large reactor over a longer time (typically hours) and with low flow velocity. Therefore, the conventional approach of using a standard volume RF coil for signal detection and exploiting thermal nuclear polarization was preferred, despite the attractive features of hyperpolarization and remote detection. An NMR compatible reactor was developed for use within a standard quadrature RF volume coil of 72 mm inner diameter. For simultaneously observing the chemical reaction and temperature changes within the reactor, an optimized pulse sequence for multislice ultrashort echo time MRSI was developed. As an example, the ethylene hydrogenation reaction was chosen. Measurements were performed for different flow rate and concentration ratios. The MRSI results were compared with mass spectrometric measurements of the products.

2. Experimental

2.1. Materials

For the preparation of Pt-Al_2O_3 catalyst, commercial cylindrical γ-Al_2O_3 pellets (length: ~8 mm; diameter: 3.2 mm; BET: 220 m^2/g; Alfa Aesar GmbH) were impregnated with a solution of water and Tetraammineplatinum(II)chloride hydrate (Sigma–Aldrich).

In a first step, the pore volume of the Al_2O_3 pellets was calculated by adding water step by step to the porous material. The amount of water, which could be completely adsorbed, was 40 % of the pellet mass. To get 1 wt.% homogeneously distributed Platinum on the pellet, Tetraammineplatinum(II)chloride hydrate was dissolved in the amount of water, which corresponds to the pore volume. After adding the platinum solution to the pellets, they were dried at 120 °C and calcined at 400 °C for 3 h. Before the experiments, the catalyst was activated at a gas flow of 2.5 Nl/min (H_2:N_2 1:5) at a temperature of 400 °C for about 2 h.

2.2. Temperature measurements

To measure the temperature level during the experiments at the inlet and outlet of the catalyst bed, cylindrical glass capsules (outer diameter 3 mm; length ca. 10 mm) were manufactured, filled with ethylene glycol (99.5 % purity, Fluka) and fused. The chemical shift difference between the —OH and —CH_2 peaks of ethylene glycol is known to correlate well with temperature within a range of 20 °C and 140 °C [26,34]. The temperature can be expressed as a function of the chemical shift difference $\Delta\delta$ in ppm [26]:

$$T(C^{\circ}) = 192.85 - 101.64\,\Delta\delta. \quad (1)$$

The ethylene glycol capsules were placed in front of and behind the reactive zone of the catalyst bed surrounded by inert Al_2O_3 pellets (cf. Fig. 1) to avoid information loss by crosstalk of the ethylene glycol signal into the gas signal. Before insertion into

Table 1
Experimental parameters (volume flow, concentration) of experiment A and B. The volumetric concentrations were measured with a pMS behind the outlet of the reactor. The concentration measurements were performed at steady state conditions. The measurement uncertainty of the pMS was for all experiments below 1%.

	Experiment A	Experiment B
$\dot{v}_{N_2}$ (Inlet)	0.175 l/min	0.4 l/min
$\dot{v}_{C_2H_4}$ (Inlet)	0.25 l/min	0.5 l/min
$\dot{v}_{H_2}$ (Inlet)	0.075 l/min	0.1 l/min
c_{N_2}	41.3 vol.%	44.2 vol.%
$c_{C_2H_4}$	40.0 vol.%	44.1 vol.%
$c_{C_2H_6}$	18.0 vol.%	11.0 vol.%
c_{H_2}	0.7 vol.%	0.7 vol.%

the catalyst bed, all capsules were tested by MRSI measurements at room temperature. Additionally, one glycol capsule was measured by the MRSI method at four constant temperature values in the range from 19 °C to 44 °C. For these measurements, the glycol capsule was inserted in a beaker filled with perfluoropolyether (Fomblin, Solvay Solexis, Bollate, Italy), in which the temperature was measured by a fiberoptic thermometer (Luxtron 504, Polytec, Waldheim, Germany). The temperature values determined from the chemical shift difference between the two NMR signals of ethylene glycol using Eq. (1) were compared with the values measured by the fiberoptic thermometer yielding a largest difference of only 0.6 K.

2.3. Ethylene hydrogenation

The investigated gas phase reaction is the hydrogenation of ethylene (see Eq. (2)). It has been chosen, because it is a well investigated reaction process [35] and offers several favorable characteristics, which makes it a good choice for a model reaction for benchmarking measurements:

$$C_2H_4 + H_2 \longrightarrow C_2H_6 \quad \Delta H_R = -137\,\text{kJ/mol} \tag{2}$$

(i) It is nearly irreversible. (ii) It can be run at ambient conditions in presence of a Pt-catalyst. (iii) It is highly exothermal like many of the industrially relevant heterogeneously catalyzed gas phase reactions. (iv) No side products are expected, which facilitates the analysis of reaction products. (v) As ethylene and ethane are symmetric molecules, both gases give rise to single resonance lines. The chemical shift difference between the two signals is larger than 4 ppm [36], which facilitates signal separation.

The reaction was run within a glass tube reactor specially designed for MRI purposes. The reactor had an inner diameter of 30 mm and the catalyst bed a length of 80 mm. The catalyst bed was structured as follows: first a 20 mm thick layer of Al_2O_3 pellets was piled up containing 3 capsules filled with ethylene glycol (cf. Fig. 1). Then a ca. 40 mm thick layer consisting of a mixture of catalytically active Pt-Al_2O_3 pellets and inert Al_2O_3 pellets were placed inside the reactor. In this layer the amount of catalytically active pellets gradually increased, beginning with very few Pt-Al_2O_3 pellets (just 2–3 in slice #2) up to 50 % of the total volume in slice #5. The last layer (thickness ca. 20 mm, including slice #6 and #7) consisted of inert Al_2O_3 pellets. In slice #7, three ethylene-glycol-capsules were placed for temperature measurements.

The supply of the reactor with nitrogen, hydrogen and ethylene was realized by mass flow controllers (F-201CV, Bronkhorst, Ruurlo, Niederlande & FMA-2618-A, Omega Engineering, Stamford, USA). The total initial volume flow varied between 0.5 l/min and 1.0 l/min with varying hydrogen content of the reactant gases (see Table 1). The outlet pressure was held at a constant level of 1.3 bar (abs). Behind the reactor outlet, the composition of the product gases was analyzed by a process mass spectrometer (pMS, GAM 200, InProcess Instruments, Bremen, Germany).

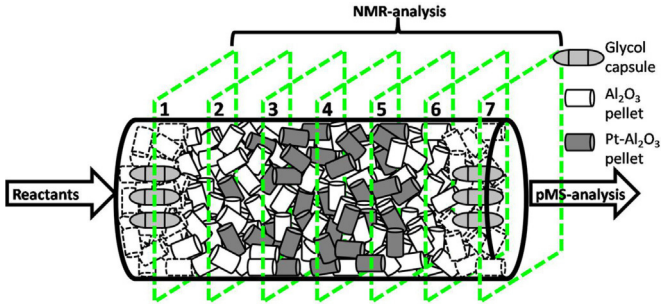

Fig. 1. Schematic representation of the structured catalyst bed: The amount of active catalyst pellets was increased from slice 2 to slice 6. The areas around slice 1 and 7 were filled with inert Al_2O_3 pellets containing 3 capsules with ethylene glycol. The slice centers were positioned at −33 mm (#1), −24 mm (#2), −14 mm (#3), −4 mm (#4), 6 mm (#5), 16 mm (#6), 30 mm (#7).

To ensure process safety and avoid any damage to the detection coil, the reactor was cooled with a steady flow of pressurized air and insulated with a glass fiber mat.

2.4. MRSI experiments

All NMR experiments were performed on a small-bore NMR imaging system Biospec 70/20 USR (Bruker Biospin MRI GmbH, Ettlingen, Germany) equipped with a horizontal 7-Tesla magnet and a magnetic field gradient insert BGA12S2 (inner diameter: 116 mm, maximum gradient strength: 441 mT/m per spatial direction, switching time: 130 μs). A quadrature birdcage RF coil with an inner diameter of 72 mm was used for both RF transmission and signal reception.

For orientation, a multislice FLASH [37] sequence was applied with the following parameters: repetition time TR: 500 ms, echo time TE: 3 ms, 31 slices, slice thickness: 2.5 mm, slice distance (center-to-center): 3 mm, field-of-view (FOV): 48 mm × 48 mm, 256 × 256 matrix size, total measurement time: 2 min 8 s. In these images, the position of the glycol containing capsules was determined, while signals from the gases were lost because of the rather long TE of 3 ms and the low gas concentration.

For the subsequent multislice MRSI experiments [38,39], the position of the outer slices (slice #1 and #7) were chosen for measuring signals from the glycol capsules, while the inner five slices were used to detect the gases (cf. Fig. 1). An optimized multislice MRSI pulse sequence was developed to realize an ultrashort echo time TE, i.e. a delay between RF excitation and data acquisition, of only 350 μs. Thus, signal losses due to short effective transverse relaxation time $T2^*$ are reduced ($S(TE) \sim \exp(-TE/T2^*)$). The asymmetric RF excitation pulse used for slice selective signal excitation was calculated by a Shinnar-Le Roux algorithm [40,41] using the module of the Vespa suite for RF pulse design (available via: http://scion.duhs.duke.edu/vespa/). The pulse was optimized for a flip angle of 30°. The pulse duration was 250 μs and the maximum was about 70 μs prior to the end of the pulse. Immediately after the RF Pulse, short triangular-shaped phase encoding gradients (130 μs switch on, 130 μs switch off), were applied for in-plane resolution using a FOV of 63 × 63 mm^2 and 42 × 42 phase encoding steps with circularly reduced k-space sampling [42]. Data acquisition was performed using 1 Ki complex data points and a spectral width of 50 kHz. Using a repetition time TR of 155 ms the total time per SI measurement was about 3.5 min. Within each TR, seven slices were sequentially measured with slice centers at −33 mm (#1), −24 mm (#2), −14 mm (#3), −4 mm (#4), 6 mm (#5), 16 mm (#6), 30 mm (#7) along the axial direction (z) of the reactor (cf. Fig. 1) with higher z values pointing from the front side into the magnet. The slice order

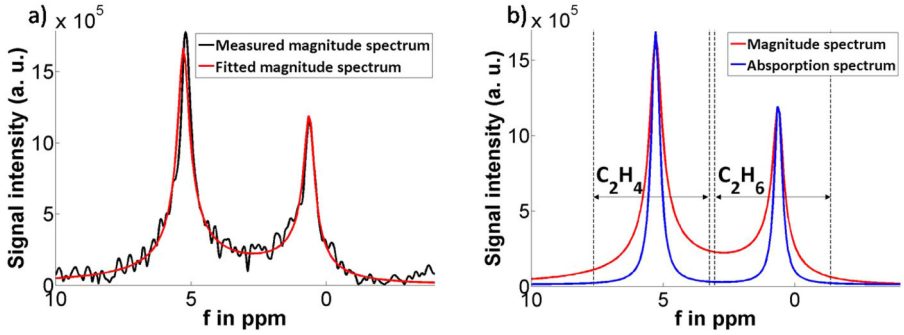

Fig. 2. (a) Typical magnitude spectrum measured of ethylene and ethane with superimposed MPM-fitted magnitude spectrum. (b) Fitted magnitude spectrum and the absorption spectrum to enhance signal separation: The signal peak of ethylene (C_2H_4) was integrated from 7.6 ppm to 3.2 ppm, the signal peak of ethane (C_2H_6) was integrated from 3.0 ppm to −1.4 ppm.

within TR was #7, #6,. . ., #1, i.e. opposite to the direction of the gas flow, to reduce saturation effects across the slices.

The temperature at the inner surface of the RF coil, measured by a fiberoptic thermometer (cf. Section 2.2), increased during the observation of the gas reaction despite the thermal insulation between gas reactor and RF coil. Therefore, tuning and matching of the RF coil were manually readjusted after the temperature had changed by 3 K. Because of these interruptions (each lasting 1–2 min), MRSI data sets were not measured at equidistant time points.

MRSI data sets were processed using in-house developed IDL (Interactive Data Language, version 7.0, Exilis Visual Information Solutions, Bolder, USA) and Matlab (version 7.11.0, The MathWorks, Inc., Natick, MA, USA) programs. The measured k-space data were apodized with a Hamming function in the phase encoding direction (kx, ky) and zero filled to a matrix size of 64 × 64 × 1 Ki. Zero filling to 8 Ki was also applied in the time domain prior to the 3D Fourier transformation (FT) of the data sets of all slices. Magnitude spectra were calculated for visual inspection of the data.

To approximate the volumetric fraction of ethylene and ethane, the peak area of both signals (I) were determined by integration, normalized by the number of attached hydrogen atoms per molecule and put into relation with each other:

$$\frac{c_{C_2H_6}}{c_{C_2H_4}+c_{C_2H_6}} \approx \frac{(I_{C_2H_6}/6)}{(I_{C_2H_4}/4)+(I_{C_2H_6}/6)}. \quad (3)$$

A simple peak area integration in the magnitude spectra was not sufficient to reliably separate the ethylene from the ethane signals. Therefore, data was fitted in each voxel using the matrix pencil method (MPM) [43], which performs data fitting in the time domain by using a sum of exponentially decaying signals each being characterized by four parameters (amplitude, frequency, phase, decaying constant). While the maximum number of signals was set to two (ethylene, ethane), the number of signals was automatically determined to account for voxels with low signal-to-noise ratio (SNR) (e.g., outside the reactor or prior to the formation of ethane). Thus, for quantitative data analysis, data processing consisted of apodization and FT in phase encoding directions, MPM in all voxels, zero filling of the fitted and phase corrected data to 8 Ki data points, and FT in the time domain. As the phases of the fitted signals were set to zero, the real part of the complex FT spectrum corresponds to the absorption spectrum yielding better signal separation than the magnitude spectrum (cf. Fig. 2). Images of the ethylene or ethane gas were calculated by peak area integration of these fitted absorption spectra. An alternative and more straightforward way for data quantification is, of course, to directly evaluate the amplitudes determined by the fitting routine. However, in individual voxels of some data sets, fitted noise peaks caused problems for the automatic signal assignment. Therefore, peak area integration in defined spectral regions of the FT spectra of the fitted time domain data was preferred to ensure a robust data quantification for the long series of 3D data sets.

For accurate temperature measurements by determining the chemical shift difference between the two glycol peaks, 8 Ki data points for a spectral width of 50 kHz are not sufficient. Therefore, the data for slices #1 and #7, were reconstructed by undersampling the time domain signal by a factor of 8 resulting in 8 Ki spectra for a spectral width of 6.25 kHz. Because of the very high SNR of the glycol signals, the corresponding SNR loss was not an issue. The straightforward alternative of zero filling to 64 Ki prior to FT would prolong data processing and may cause memory problems of the computer.

3. Results and discussion

The hydrogenation experiments were performed at different flow rates and initial hydrogen concentrations (cf. Table 1). Fig. 3 shows a typical map of spectra measured during steady state operation mode in the middle of the catalyst bed. Only the inner 42 × 42 spectra of the reconstructed 64 × 64 matrix are shown to maintain visibility of the single spectra. Additionally, the spectra are scaled up by a factor of two to improve readability of spectra with broad resonance lines resulting from low B0 homogeneity.

The map clearly shows the circular cross section of the catalyst bed. Despite intensity differences of up to a factor of ten, all voxels within the cross section are analyzable. The intensity differences arise from B0 field inhomogeneities due to varying composition of the catalyst bed and temperature gradients along the cross section of the reactor. The chemical shift difference between the peaks of ethylene and ethane are in accordance with the expected values reported in literature [36]. During all experiments neither significant shifts of the peak positions nor exaggerated peak broadening was observed (cf. Figs. 2–4). Outside the catalyst bed just noise is detected apart from a small circular area beneath the catalyst bed. We assume that this signal arises from small amounts of condensed water steam which could be carried by the pressurized air of the cooling circuit. Thus, the map of spectra and the achieved SNR clearly show that in spite of reactant flow conditions slice selective excitation and in-plane resolution by phase encoding is feasible by using the optimized ultrashort TE MRSI pulse sequence.

To demonstrate that it is possible to detect the reaction progress along the catalyst bed, Fig. 4 shows single spectra of the 5 inner slices at the same voxel position along the longitudinal axis of the reactor. It can be seen that the MPM fitting algorithm performs well in regard to the application case: The NMR signals are fitted as single peaks, however, only if the signal exceeds the noise level to a

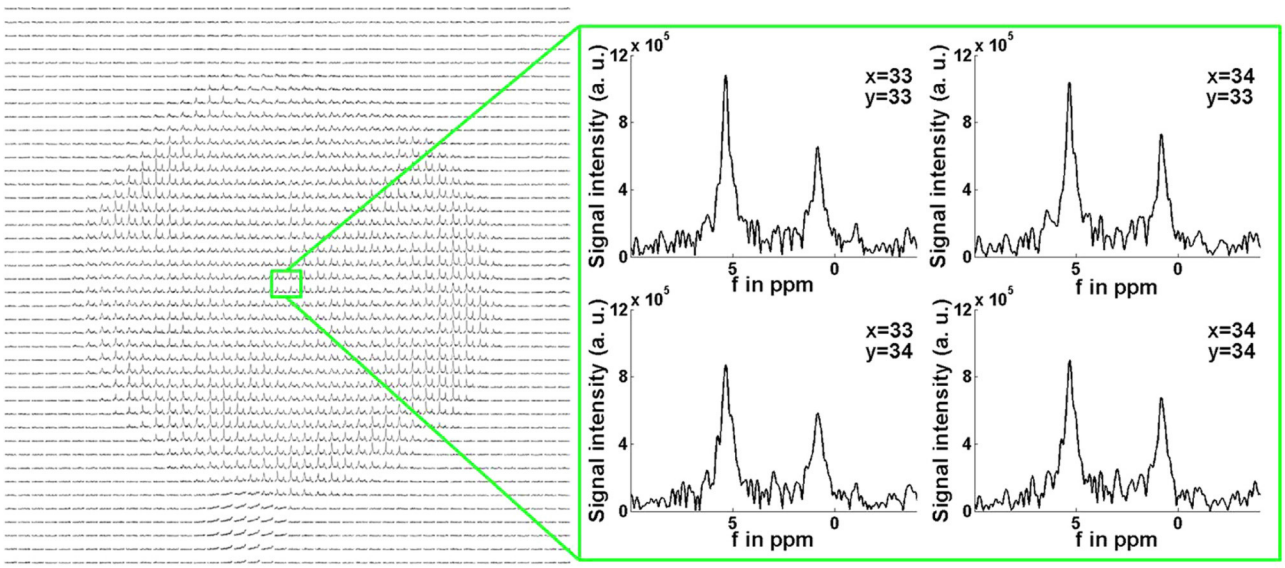

Fig. 3. Representative spectral map measured at steady state conditions: for improved readability only the inner 42 × 42 spectra of the measured 64 × 64 matrix is shown and the spectra are scaled up by a factor of 2.

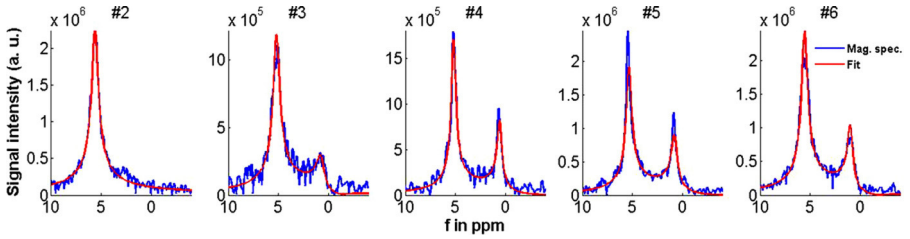

Fig. 4. Single spectra of the 5 inner slices (a–e from left to right) at the same voxel position along the longitudinal axis of the reactor at reaction conditions with superimposed MPM-fits.

certain extent (cf. Fig. 4a and b). For automatically determining the number of peaks, the AIC criterion of the MPM algorithm performed better than the MDL criterion [43], because the latter tended to miss peaks at lower SNR.

The progress of the reaction can be tracked along the spectra: in Fig. 4a no ethane peak could be spotted. The ethane signal appears the first time in Fig. 4b, increases in Fig. 4c and stays stable in Fig. 4d and e. The variation corresponds to the expected reaction progress along the catalyst bed.

Beside the variation of the peak ratios significant differences in signal intensity along the longitudinal axis of the reactor are noticeable. To investigate the signal intensity pattern, the peak areas of ethylene and ethane were added and plotted along the horizontal plane of symmetry. The resulting signal intensity profile of an experiment detected under steady state conditions (Experiment A, cf. Table 1) is shown in Fig. 5. The signal intensity profile of a single slice shows significant similarities to the profile along all slices: both increase from the inside to the outside. This can be explained by the corresponding temperature profile along the axial and the radial direction of the catalyst bed: Due the structure of the catalyst bed, the conversion is mainly expected to take place within slices #3–#5 and thus leading to higher temperature levels than in slices #2 and #6. Additionally, the peripheral zones of the catalyst bed are cooled by the cooling circuit. Both effects lead to u-shaped temperature profiles along the radial and longitudinal axis of the catalyst bed. Considering that the nuclear magnetization of a sample decreases with increasing temperature due to the Boltzmann distribution ($M_0 \sim \exp(-\Delta E/kT)$ with ΔE being the difference between the adjacent energy levels, k the Boltzmann constant and T the absolute temperature), the signal intensity should be lower in areas of elevated temperature.

Furthermore, the effect of isobaric conditions of the hydrogenation process has to be considered. In areas of elevated temperatures, the gas density and thus the spin density drops leading to an additional signal decrease. In the data set used Fig. 5, the averaged total

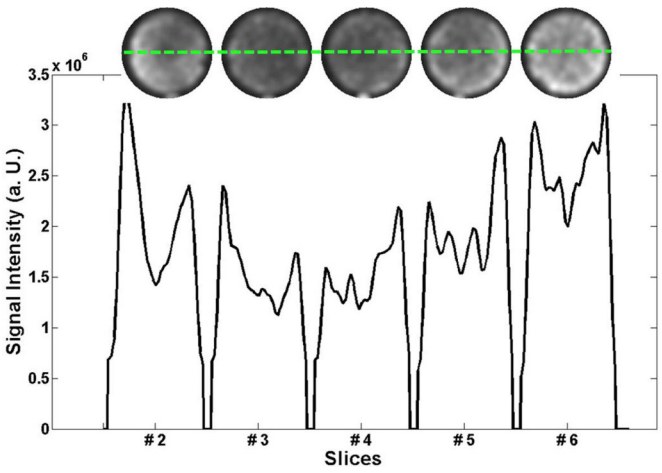

Fig. 5. Signal intensity of the sum of the peak area of ethylene and ethane added and plotted along the horizontal plane of symmetry.

signal intensities of slice #2 and slice #4 differ by about 24 %. The temperature difference measured with a thermal couple at comparison measurements outside the reactor yielded about 45 K (110 °C, 65 °C; data not shown). If one calculates the expected intensity loss caused by decreased nuclear magnetization and density loss (assumption: ideal gas) alone, one would expect a signal difference of about 22%. However, at least two further aspects have to be considered when explaining the observed regional differences in the NMR signals. First, for the MRSI pulse sequence used, the protons of the H_2 gas are NMR invisible due to the very short T2* relaxation time (e.g., T2* ~ 200 μs measured in separate experiments in a gas mixture of H_2 and CH_4 at room temperature, data not shown) and the strong diffusion [44] during the slice selective RF pulse causing dephasing of the transverse magnetization. However, as part of the ethane molecule they become NMR visible and contribute to the measured spectra. Second, the T1 and T2 relaxation times may also be temperature dependent and could thus influence the observed signal profiles across the reactor because of saturation effects and signal losses during the echo time TE.

3.1. Temperature measurements

Knowledge about the temperature conditions within a catalyst bed is crucial to evaluate process performances. To get information about inlet and outlet temperature of the catalyst bed, the spectra of ethylene glycol were measured in slices #1 and #7 by the multislice MRSI pulse sequence. As outlined above, the time domain data was fitted by the MPM algorithm and the absorption-like spectra were used for determining the chemical shift difference.

At least 16 ethylene glycol spectra of each capsule could be detected. The inner four spectra were used for temperature determination and the values were averaged (cf. Fig. 6a). The resulting temperatures corresponded well to those measured with conventional thermocouples during comparison measurements outside the magnet. The temporally resolved temperature profiles of two experiments are shown in Fig. 6b. The experiments A and B differ in regard to the volume flow and hydrogen content of the reactant gas (see. Table 1). As expected, the temperature profiles of both experiments differ considerably. The inlet temperature of experiment A is higher than the outlet temperature, with the difference being lower than 10 K. Opposite conditions are found in experiment B: Here the inlet temperature just increases slightly, whereas the outlet temperature is more than 50 K higher. The opposing temperature profiles are to be expected, because on the one hand the lower flow rate of experiment A promotes compensatory diffusional processes, which lead to lower temperature gradients. On the other hand the higher flow velocity of experiment B shifts the reactive zone, and thus higher temperatures, towards the outlet of the catalyst bed. These results demonstrate that the ethylene glycol capsules respond sensitively enough to temperature changes to map the temperature profiles within a catalyst bed. Due to the dimensions of the capsules, which are in the same order of magnitude as the catalyst pellets, we further assume no significant distortion impact on the flow pattern of the reactant gases.

As the gas composition was simultaneously measured in slices #2–#6, this multislice MRSI approach yields information both on the spatial distribution of gases and on the temperature in the reactor. In the alternative case of temporally alternating measurements of gas distribution and temperature, one could perform the temperature measurements by volume selective spectroscopy measurement as demonstrated by Gladden et al. [27] in well defined voxels, allowing optimized shim values, i.e. better local B0 homogeneity. However, using the global shim values used for multislice MRSI allowed precise and reproducible temperature measurements (cf., Fig. 6). Therefore, the integration of gas distribution and temperature measurements within a multislice MRSI sequence was preferred to avoid any time delay between gas and temperature measurements.

Table 2
Results of the averaged volumetric concentration of ethane of experiment A and B measured by MRSI and pMS.

	Experiment A		Experiment B	
	t = 1 :31 : 52 h	t = 1 :43 : 15 h	t = 1 :13 : 52 h	t = 1 :21 : 29 h
Slice 5	16.1 vol.%	16.4 vol.%	9.8 vol.%	9.5 vol.%
Slice 6	14.4 vol.%	14.5 vol.%	10.0 vol.%	10.2 vol.%
pMS	18.0 vol.%	18.0 vol.%	11.0 vol.%	11.0 vol.%

3.2. Gas composition measurements

To estimate the gas composition in every voxel, the hydrogen conversion was calculated based on the ratio of the ethane peak area normalized to the number of attached hydrogen molecules divided by the sum of the normalized peak areas of ethane and ethylene (see Eq. (3)). In each voxel, this ratio of normalized peak areas corresponds to the ratio between the volumetric concentration ethane and the sum of the volumetric concentrations of ethylene and ethane.

In pMS measurements only insignificant amounts of hydrogen were found at the outlet (Table 1). With this information the NMR pattern could be quantified in terms of hydrogen conversion X_{H_2}:

$$\frac{c_{C_2H_6}}{c_{C_2H_4} + c_{C_2H_6}} \cdot \alpha \approx X_{H_2}, \tag{4}$$

where α is a proportionality constant which can be calculated from the ratio of ethane concentration to the sum of ethylene and ethane concentration at a known hydrogen conversion. Here the factor α was calculated based on the concentration conditions at the outlet measured by the pMS. By taking the inlet conditions into account (cf. Table 2), balance equations of each component, depending on the hydrogen conversion, can be set up:

$$\dot{v}_i = \dot{v}_{i,0} + \nu_i X_{H_2} \cdot \dot{v}_{H_2,0}, \tag{5}$$

where i refers to the chemical components present in the system (N_2, H_2, C_2H_4,C_2H_6), 0 indicates the inlet conditions, $\dot{v}_i$ is the corresponding volume flow, and ν_i the stoichiometric factor of component i. Thus the volumetric concentration of ethane can be calculated in each voxel. The resulting concentration distribution of ethane for experiments A and B are shown in Figs. 7 and 8, respectively.

For both experiments the spatial distribution of ethane is shown for four different points in time:

(a) Only nitrogen and ethylene are flowing through the reactor. No hydrogenation should take place
(b) Hydrogen is switched on. First measurement at transient reaction conditions
(c) Measurement at steady state conditions as assumed from the temperature profile (Fig. 6)
(d) Comparison measurements at steady state conditions

The corresponding temperature measurements are shown in Fig. 6 and the time points used for the data presented in Fig. 7 and 8 are marked with red circles. The results of experiment A show clearly that a good signal separation is achieved by fitting and phase correcting the signal: nearly no ethane is detected within the slices at t = −5 min. The next set of measurements (Fig. 7b) presents the ethane concentration at transient reaction conditions: First small amounts of ethane can be detected in slice #3 and are increasing towards the outlet of the catalyst bed. A detailed quantification of these amounts is not useful because the hydrogen conversion

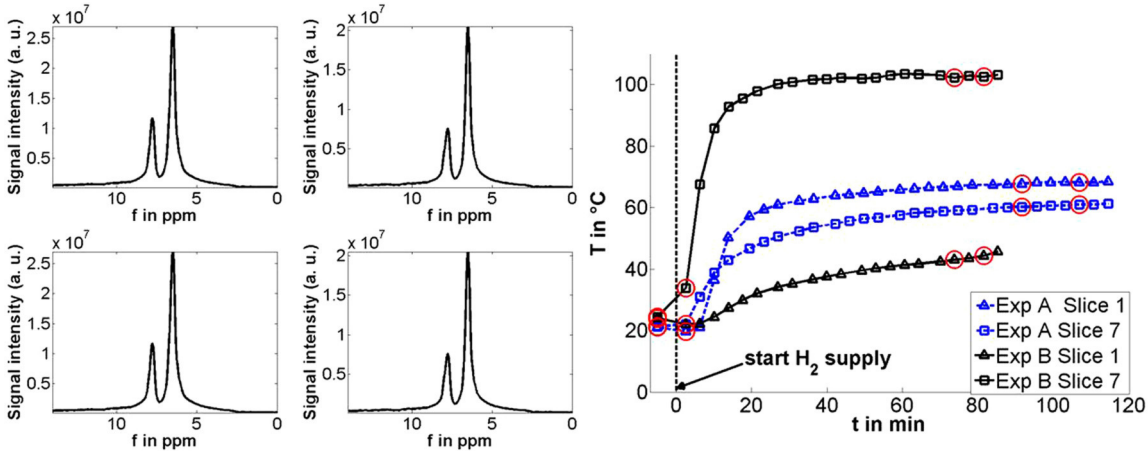

Fig. 6. Temperature profiles of the inlet and outlet of the catalyst bed of experiment A and experiment B. The temperatures were averaged over the four inner ethylene glycol spectra of the central capsule. All time information corresponds to the middle of the measurement duration.

increased from 0 % to 80 % during the measurement time of about 3.5 min. The ethane concentration profile of a steady state measurement can be seen in Fig. 7c. First locally limited zones with elevated ethane concentration can be detected in slice #2. Shape and position of these zones within the catalyst bed correspond to shape and position of single Pt-Al_2O_3 pellets that are surrounded by inert Al_2O_3 pellets which were inserted there.

With increasing ratio of catalyst pellets from slice #2–#4 the number of active zones of the catalyst bed increase, but in all cases the active zones can still be clearly separated from each other. Thus

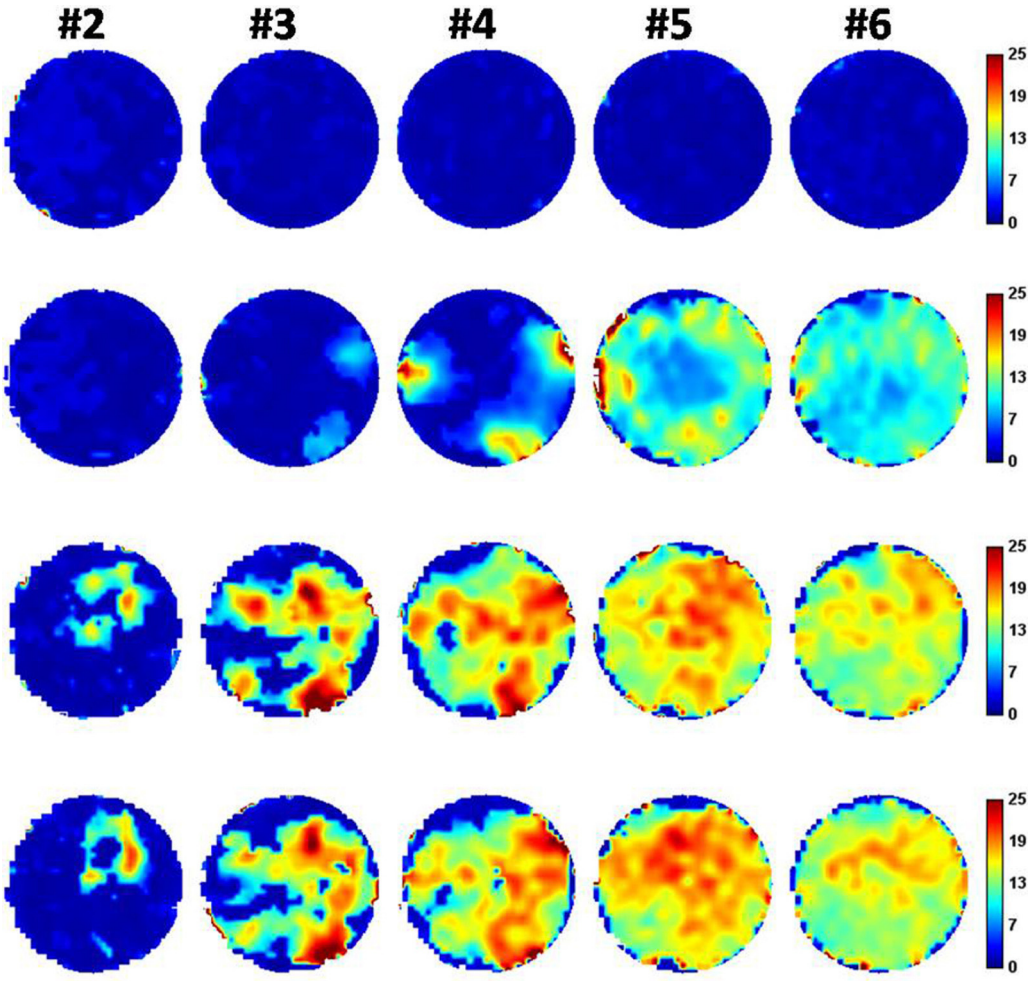

Fig. 7. Volumetric concentration maps of ethane of experiment A given in vol.%. The measurements (a–d from top to bottom) were performed at (a) $t = -5$ min, (b) $t = 2:30$ min, (c) $t = 1:31:52$ h, and (d) $t = 1:43:15$ h; all time information corresponds to the middle of the measurement duration.

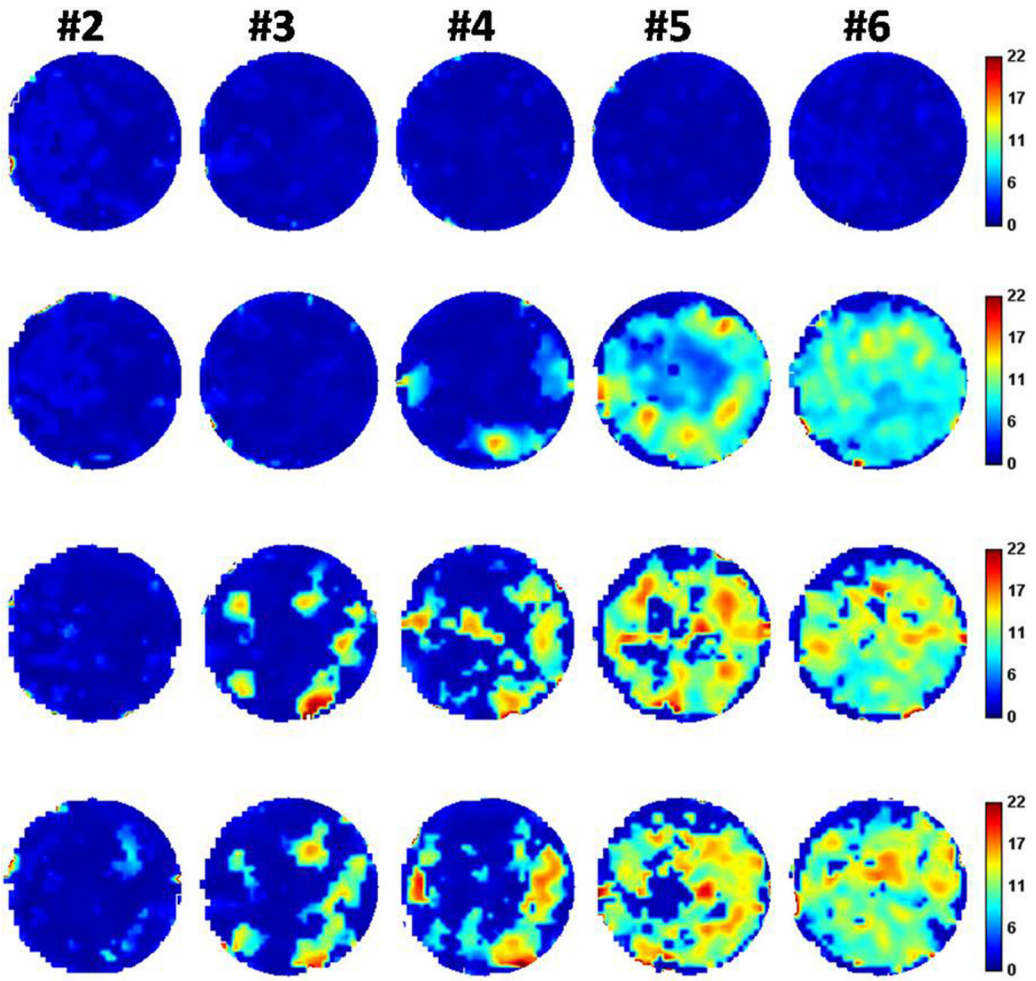

Fig. 8. Volumetric concentration maps of ethane of experiment B given in vol.%. The measurements (a–d from top to bottom) were performed at (a) $t = -5$ min, (b) $t = 2:30$ min (c) $t = 1:13:52$ h and (d) $t = 1:21:29$ h; all time information corresponds to the middle of the measurement duration.

it can be assumed that the zones of elevated ethane concentration are the active zones of the catalyst bed. Along the next two slices the amount of ethane increases, whereas the concentration gradients along the cross section decrease.

Slice #6 shows the most homogeneous concentration distribution. The concentration gradients are less pronounced compared to the previous slices. This reflects that a homogenization by mixing of the gases within the inert layer is achieved.

The similarity of pattern in Fig. 7c and d confirm the steady state assumption. Active zones can be detected at similar locations of the catalyst in all the slices. This demonstrates the reproducibility of the MRSI measurements.

Surprisingly, it appears that the averaged concentration of ethane decreases from slice #5 to slice #6. If one compares the averaged ethane concentration of slices #5 and #6, the apparent decrease of ethane content is confirmed (cf. Table 2). Whereas the averaged volumetric ethane concentration of slice #5 corresponds to the pMS measurements better than 90%, the correspondence drops in slice #6 to 80%. This can not be explained by an actual decrease of ethane, because the reverse reaction does not occur at the present reaction conditions and the pMS measures the gas composition behind the outlet of the reactor. This effect was also detected in different experiments with the same volume flow but varying hydrogen contents (data not shown).

We hypothesize an NMR artifact, caused by saturation effects, leads to the apparent ethane decrease. With increasing slice index (in flow direction) the probability increases that spins that are to be measured have already been measured at an earlier time point in an adjacent slice. In particular, this applies to the ethane signal, which is only formed in the center of the reactor, and could thus suffer saturation. Thus an increasing percentage of ethane could be partially saturated, causing a signal decrease. However, we tried to minimize saturation effects by using 30° excitation pulses and measuring slices of 3 mm thickness with 10 mm center-to-center distance. In future experiments, we plan to examine the influence of saturation effects by performing single slice MRSI or using multislice MRSI with longer repetition time. Additionally, measurements of the T1 relaxation times of the gases will help to estimate saturation effects.

The results of experiment B (Fig. 8a–d) demonstrate the influence of flow rate on spatial and temporal differences in the volumetric ethane concentration. In this experiment, the signal level of ethane is lower because of the lower hydrogen content in the reactant gas flow and the higher temperature in the reaction zones (cf. Fig. 6) resulting from the higher flow velocity. Due to the lower SNR compared to experiment A, the fitting procedure failed to find an ethane peak in some voxels, particularly in slices #2 and #3. Nevertheless the experiment could be analyzed allowing the observation of the temporal and regional development of the ethane concentration in the reactor. Compared to Experiment A the reactive zones are shifted towards the outlet of the catalyst bed. This corresponds to the temperature profiles of Fig. 6.

Apart from the lower amount of ethane present in the system, the active zones of the catalyst bed of experiment A and experiment B follow comparable pattern: The active zones of the transient measurement of experiment B are in the same position as in experiment A (cf. Fig. 7b with Fig. 8b, slices #3 and #4). The stationary measurements show also comparable active zones at the same position (cf. slice #3 and #4 of Fig. 7c and d and slice #3 and #4 of Fig. 8c and d). In accordance with experiment A both steady state measurements are comparable with each other. Both measurements show similar reaction zones and the averaged volumetric ethane contents of slices #5 and #6 deviate only slightly from each other (see Table 2), which underlines the reproducibility of the measurements.

The major difference between experiment A and experiment B is that in experiment B no decrease of ethane content between slices #5 and #6 was detected. The averaged volumetric ethane content of slice #6 corresponds to the pMS measurements better than 90%. This might be a hint that saturation effects are the main reason for the apparent ethane decrease. Due the fact that the reaction zone is shifted towards the outlet of the catalyst bed, more ethane is produced between slices #5 and #6 and thus the extend of ethane saturation is lower than in experiment A, leading to lower deviation from the ethane concentration measured with the pMS. Nevertheless this effect will be addressed in the next experimental campaign as discussed above. Alternatively, measurements on non-reactive ethane/ethylene flows may help to explain why differences in the volumetric ethane concentrations between slices #5 and #6 were observed in experiment A, but not in experiment B.

4. Conclusion

The presented results prove that optimized ultrashort echo time multislice MRSI can successfully be applied to analyze heterogeneously catalyzed gas phase reaction systems at ambient conditions, despite the disadvantageous NMR properties of gaseous flows. Using the hydrogenation of ethylene as benchmark process, simultaneous spatial mapping of the chemical composition was demonstrated within five 3-mm-slices across a model reactor, an in-plane resolution of about 1.5 mm, and a time resolution of about 3.5 min. It was possible to clearly and reproducibly identify the active zones of a catalyst bed, to follow the progress of the reaction along its longitudinal axis, and to separate and quantify the observed gases by using the matrix pencil method, a fast and robust time domain fitting algorithm. Further the multislice MRSI method allows to simultaneously measure the temperature within the catalyst bed. Expected temperature changes could be observed immediately in front of and after the active reaction zone, and characteristic differences between measurements with different hydrogen content and different volume flow were detected. Therefore, we are confident that ultrashort TE multislice MRSI will be a powerful tool for optimizing heterogeneously catalyzed gas phase processes in model reactors and for validating modeling approaches.

There are certainly also a number of general disadvantages and technical challenges of the presented methodology. Compared to other methods used for NMR signal enhancing like remote detection or hyperpolarization, the presented approach suffers from lower SNR, particularly for higher temperatures. Nevertheless, it may be a method of choice for investigating gas phase reaction systems of larger macroscopic scale over longer time periods, because the experimental effort and the costs are rather low compared to approaches exploiting hyperpolarization, and the methods can be applied for slow flow through long reactors, unlike techniques using remote detection.

Additionally, the implemented method can be improved in several ways. Thus, an SNR increase will be possible if excitation RF pulses with optimized flip angle will be used based on knowledge on T1 relaxation times and flow velocities. A further reduction of the echo time can be achieved, either by methodological improvements or improved hardware components, particularly faster B0 gradients. Furthermore, data processing and quantification can be improved by adjusted and optimized procedures, e.g. by using prior knowledge about the chemical shifts.

The development of new NMR compatible reactors should focus on enabling measurements at higher temperature and higher pressure. Additionally, improving the thermal insulation and or the cooling of the outer reactor wall will be essential to avoid readjustments of the RF coil, and to allow a smaller distance between reactor and RF coil, thus yielding a higher filling factor and consequently a higher SNR.

We hope that the described methodology and the presented results will foster the application MRSI methods to investigate other heterogeneously catalyzed gas phase reaction systems and encourage multidisciplinary cooperation between researchers focusing on chemical engineering and NMR imaging methods.

Acknowledgment

We would like to thank Roswita Krebs-Goldbecker from the glass workshop of the University of Bremen for her obliging assistance with the manufacturing of the experimental setup. This work was in part supported by the German Research Foundation (DFG) within the Research Training Group GRK 1860 “Micro-, meso- and macroporous nonmetallic Materials: Fundamentals and Applications” (MIMENIMA).

References

[1] M. Boudart, B. Davis, H. Heinemann, in: G. Ertl, H. Knözinger, F. Schüth, J. Weitkamp (Eds.), Handbook of Heterogeneous Catalysis, Wiley-VCH Verlag GmbH, 2008, pp. 1–48.
[2] J. LePage, R. Schlögl, M. Wainwright, F. Schü, K. Unger, E. Ko, H. Jacobsen, P. Kleinschmit, R. Menon, B. Delmon, K.-Y. Lee, M. Misino, S. Oyama, in: G. Ertl, H. Knözinger, F. Schüth, J. Weitkamp (Eds.), Handbook of Heterogeneous Catalysis, Wiley-VCH Verlag GmbH, 2008, pp. 49–138.
[3] R. Heck, S. Gulati, R. Farrauto, Chem. Eng. J. 82 (2001) 149–156.
[4] J. Chen, H. Yang, N. Wang, Z. Ring, T. Dabros, Appl. Catal. A: Gen. 345 (2008) 1–11.
[5] E. Tronconi, G. Groppi, C. Visconti, Curr. Opin. Chem. Eng. 5 (2014) 55–67.
[6] T. Schildhauer, K. Pangarkar, J. van Ommen, J. Nijenhuis, J. Moulijn, F. Kapteijn, Chem. Eng. J. 185–186 (2012) 250–266.
[7] D. Vervloet, F. Kapteijn, J. Nijenhuis, J. van Ommen, Chem. Eng. J. 233 (2013) 265–273.
[8] I. Graef, A.-K. Rühl, B. Kraushaar-Czarnetzki, Chem. Eng. J. 244 (2014) 234–242.
[9] J. Mantzaras, Flow Turbul. Combust. 90 (2013) 681–707.
[10] A. Schneider, J. Mantzaras, R. Bombach, S. Schenker, N. Tylli, P. Jansohn, Proc. Combust. Inst. 31 (2007) 1973–1981.
[11] E. Gross, X.-Z. Shu, S. Alayoglu, H. Bechtel, M. Martin, F. Toste, G. Somorjai, J. Am. Chem. Soc. 136 (2014) 3624–3629.
[12] A. Zellner, R. Suntz, O. Deutschmann, Angew. Chem. Int. Ed. 54 (2015) 2653–2655.
[13] F. Zaera, Chem. Soc. Rev. 43 (2014) 7624–7663.
[14] I.V. Koptyug, in: J. Yarwood, R. Douthwaite, S. Duckett (Eds.), Spectroscopic Properties of Inorganic and Organometallic Compounds, vol. 45, The Royal Society of Chemistry, 2014, pp. 1–42.
[15] L. Gladden, Curr. Opin. Chem. Eng. 2 (2013) 331–337.
[16] S. Stapf, S.-I. Han, NMR Imaging in Chemical Engineering, John Wiley & Sons, 2006.
[17] A. Abragam, M. Goldman, Rep. Prog. Phys. 41 (1978) 395.
[18] C. Bowers, D. Weitekamp, J. Am. Chem. Soc. 109 (1987) 5541–5542.
[19] A. Moulé, M. Spence, S.-I. Han, J. Seeley, K. Pierce, S. Saxena, A. Pines, Proc. Natl. Acad. Sci. U. S. A. 100 (2003) 9122–9127.
[20] J. Seeley, S.-I. Han, A. Pines, J. Magn. Reson. 167 (2004) 282–290.
[21] I. Koptyug, A. Lysova, A. Kulikov, V. Kirillov, V. Parmon, R. Sagdeev, Appl. Catal. A: Gen. 267 (2004) 143–148.
[22] L. Gladden, M. Mantle, A. Sederman, Adv. Catal. 50 (2006) 1–75.
[23] L. Gladden, B. Akpa, L. Anadon, J. Heras, D. Holland, M. Mantle, S. Matthews, C. Mueller, M. Sains, A. Sederman, Chem. Eng. Res. Des. 84 (2006) 272–281.
[24] I. Koptyug, A. Lysova, R. Sagdeev, V. Parmon, Catal. Today 126 (2007) 37–43.
[25] A. Lysova, I. Koptyug, A. Kulikov, V. Kirillov, R. Sagdeev, Top. Catal. 52 (2009) 1371–1380.
[26] A. Van Geet, Anal. Chem. 40 (1968) 2227–2229.

[27] L. Gladden, F. Abegão, C. Dunckley, D. Holland, M. Sankey, A. Sederman, Catal. Today 155 (2010) 157–163.
[28] L. Bouchard, S. Burt, M. Anwar, K. Kovtunov, I. Koptyug, A. Pines, Science 319 (2008) 442–445.
[29] K. Kovtunov, I. Beck, V. Zhivonitko, D. Barskiy, V. Bukhtiyarov, I. Koptyug, Phys. Chem. Chem. Phys. 14 (2012) 11008–11014.
[30] V. Zhivonitko, V.-V. Telkki, J. Leppaniemi, G. Scotti, S. Franssila, I. Koptyug, Lab. Chip 13 (2013) 1554–1561.
[31] S. Roberts, M. Renshaw, M. Lutecki, J. McGregor, A. Sederman, M. Mantle, L. Gladden, Chem. Commun. 49 (2013) 10519–10521.
[32] C. Jameson, Chem. Rev. 91 (1991) 1375–1395.
[33] P. Glover, P. Mansfield, Rep. Prog. Phys. 65 (2002) 1489–1511.
[34] C. Ammann, P. Meier, A. Merbach, J. Magn. Reson. 46 (1982) 319–321.
[35] F. Zaera, G. Somorjai, J. Am. Chem. Soc. 106 (1984) 2288–2293.
[36] H. Ebrahimi, H. Shaghaghi, M. Tafazzoli, Conc. Magn. Reson. A 38A (2011) 269–279.
[37] A. Haase, J. Frahm, D. Matthaei, W. Hänicke, K.-D. Merboldt, J. Magn. Reson. 213 (2011) 533–541.
[38] T. Brown, B. Kincaid, K. Ugurbil, Proc. Natl. Acad. Sci. U. S. A. 79 (1982) 3523–3526.
[39] A. Maudsley, S. Hilal, W. Perman, H. Simon, J. Magn. Reson. 51 (1983) 147–152.
[40] M. Shinnar, L. Bolinger, J. Leigh, Magn. Reson. Med. 12 (1989) 88–92.
[41] J. Pauly, P. Le Roux, D. Nishimura, A. Macovski, IEEE Trans. Med. Imaging 10 (1991) 53–65.
[42] A. Maudsley, G. Matson, J. Hugg, M. Weiner, Magn. Reson. Med. 31 (1994) 645–651.
[43] Y.-Y. Lin, P. Hodgkinson, M. Ernst, A. Pines, J. Magn. Reson. 128 (1997) 30–41.
[44] T. Marrero, E. Mason, J. Phys. Chem. Ref. Data 1 (1972) 3–118.